archives
of thermodynamics
Vol. **44**(2023), No. 1, 63–87
DOI: 10.24425/ather.2023.145877

Heat transfer and friction characteristics in three-side solar air heaters with the combination of multi-v and transverse wire roughness

DHANANJAY KUMAR*

B.A. College of Engineering and Technology, Ghutia, P.O. Barakhurshi
Jamshedpur, Jharkhand 832304, India

Abstract The present paper describes the experimental analysis of heat transfer and friction factor for glass protected three-side artificially roughened rectangular duct solar air heaters (SAHs) having an arrangement of multiple-v and transverse wires (top wall multi-v and two side walls transverse) under the absorber plate, and compares their performance with that of one-side roughened solar air heaters under similar operating conditions. The investigated three-side solar air heaters are characterized by a larger rate of heat transfer and friction factor as compared to one-side artificially roughened SAHs by 24–76% and 4–36%, respectively, for the identical operating parameters. The air temperature below the three-side rugged duct is by 34.6% higher than that of the one-side roughened duct. Three-side solar air heaters are superior as compared to one-side artificially roughened solar air heaters qualitatively and quantitatively both.

Keywords: Absorber plate; Fluid flow; Heat transfer; Solar air heater; Reynolds number; Relative roughness height

Nomenclature

A_o	–	area of orifice plate m^2
A_p	–	area of absorber plate, m^2
H	–	depth of the duct, m

*Corresponding Author. Email: dhananjaykumar84nit@gmail.com

C_p	–	specific heat of air at constant pressure, J/kgK
D_h	–	hydraulic diameter of solar air heater, $= 4WH/2(W+H)$, m
d/w	–	relative gap position
e	–	artificial roughness height, m
f_r	–	average friction factor
e/D_h	–	relative roughness height
g	–	gravitational acceleration, m/s^2
h	–	convective heat transfer coefficient, W/m^{2}K
Δh_1	–	difference in height of U-tube manometer fluid column, m
Δh_2	–	difference in height of micromanometer fluid column, m
I	–	intensity of solar radiation, W/m^2
k	–	thermal conductivity of air, W/m K
L	–	length of test section, m
$\dot{m}$	–	mass flow rate of air, kg/s
Nu_r	–	average Nusselt number
P	–	roughness pitch, m
Q_u	–	heat gain, W
P/e	–	relative roughness pitch
ΔP_O	–	pressure difference in U-tube manometer, Pa
ΔP_d	–	pressure difference in micromanometer, Pa
Re	–	Reynolds number
t_a	–	ambient temperature, K
t_i	–	inlet air temperature, K
t_O	–	outlet air temperature, K
t_p	–	average plate temperature, K
t_f	–	average air temperature, K
Δt	–	change in temperature, K
V	–	velocity of air inside the duct, m/s
W	–	width of duct, m
w	–	roughness width, m
W/H	–	duct aspect ratio
W/w	–	relative roughness width

Greek symbols

α	–	angle of attack, degree
β	–	ratio of orifice diameter to pipe diameter
ρ	–	density of air, kg/m^3
ρ_1	–	density of fluid used in U-tube manometer, kg/m^3
ρ_2	–	density of fluid used in micromanometer, kg/m^3
μ	–	dynamic viscosity of the air, kg/ms

Subscripts

$1r$	–	one side roughened duct
$3r$	–	three side roughened duct

1 Introduction

The thermal performance of a traditional solar air heater (SAH) is generally deficient due to a low rate of convective heat transfer between the absorber plate and air flowing in the duct. The low convective heat transfer coefficient is normally attributed to the occurrence of a viscous sub-layer, which can be broken by providing synthetic roughness on the air flow side of the absorber plate [1, 5, 6]. This creates turbulence in flow, so the effect of thermal resistance reduces and the heat transfer rate becomes enhanced [7, 10]. Solar air collector is a device in which the air is delivered through a four-sided cross-section duct underneath a metallic absorber plate with its sun-facing side black coated to enable immersion of incoming solar radiation and convert it into thermal energy. The glass shield is placed over the rectangular duct to reduce the convective and radiative losses [11–15]. The animated air is used for numerous applications such as space warming, crop drying, seasoning of timber and industrial purpose [16–18]. A schematic representation of a conventional SAH is illustrated in Fig. 1.

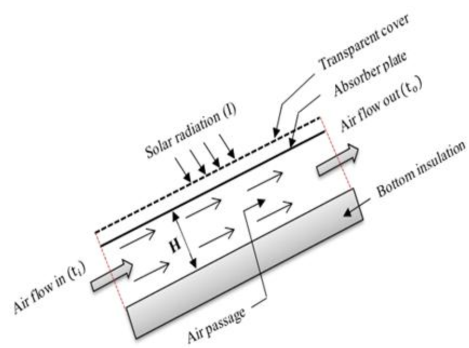

Figure 1: Schematic representation of traditional SAH.

The number of experimental and theoretical inquiries has been authorized by many investigators with fabricated roughness geometries on the absorber plate of the SAH duct [19–21]. The fabricated roughness was applied on a single side, double sides or three-sides of the absorber plate walls. Karwa and Chitoshiya made a tentative analysis of thermo-hydraulic performance of SAH with 60° v-down discrete rib roughness on the air-flow side of the absorber plate along with that of plain SAHs [22]. Kumar *et al.* [23] established the results of investigations of the effect of multi v-shaped ribs with gap roughness in one broad wall and found that an increase in the Nusselt number and friction factor as compared to plain SAHs can be 6.74

and 6.37 times, respectively. Maithani and Saini made attempts to increase the heat transfer factor of a SAH duct roughened in the form of v-shaped ribs through regular gaps as turbulence promoters [24]. Gupta *et al.* [25] installed the inclined ribs as an inclined state which carried greater thermal enactment as related to a transverse and flat plate SAH duct; they also evaluated the thermohydraulic enactment analytically. Deo *et al.* [26] made investigations using multi-gap v-down ribs joined through staggered ribs on the major wall, i.e. on the absorber plate of SAH. Prasad *et al.* [27] analytically inspected the impact of transverse round wire ribs as a fabricated roughness three-side rugged SAH duct, and reported that it is superior as compared to one-sided transverse ribs. Using a mathematical model, the thermal and effective efficiency aspect of discrete v-down rib roughness was inspected by Singh *et al.* [28]. Behura *et al.* [21] experimentally explored the characteristics of heat transfer, friction factor and thermal enactment of an innovative type of three-side artificially roughened SAH with lead crystal shield under completely developed turbulent flow circumstances and stated that three-side artificially roughened SAHs are grander to those of one-side roughened SAHs qualitatively and quantitatively both. Kumar *et al.* [31] empirically inspected the influence of geometrical restrictions of multi v-shaped ribs with a gap on heat transfer and fluid flow characteristics of a four-sided duct SAH over an animated plate having rib roughness on its underneath and found that the maximum increase in the Nusselt number and friction factor are 6.32 and 6.12 times with respect to that of a plain duct, respectively. Different types of rib arrangements are revealed in Table 1.

In this exploration, innovative roughness geometry *viz.* an alignment of multiple-v and transverse wire roughness is recommended for tentative inquiry in a SAH with parallel boundary conditions. The main intentions of the present investigations are:

I. To review the effect of relative roughness pitch (P/e), and relative roughness height (e/D_h) at varying values of Reynolds number (Re) on the heat transfer and friction factor of SAH roughened with three-side (top wall multi-v and two side walls transverse) wire with the existing roughness geometry and compare with the values acquired applying the one-side roughened duct to estimate the improvement in enactment of the solar air heaters.

II. To compare the heat transfer and friction factor for the offered roughness outline of three-side roughened SAHs with other greatest performing outcomes of the multiple-v ribs roughness as stated by Hans *et al.* [30].

III. To recommend the best performing configurations and inspect roughness geometry limitations.

Table 1: Distinct types of rib arrangements

Arrangement	Roughness limitations	Roughness geometry	Reference
Transverse continuous ribs	$P/e = 10–20$ $e/D_h = 0.020–0.033$ Re = 5000–50000	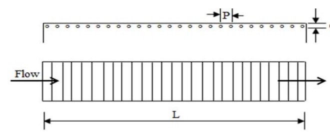	Prasad and Saini [15]
Inclined continuous ribs	$P/e = 10$ $e/D_h = 0.020–0.053$ $W/H = 6.8–11.5$ $\alpha = 30°–90°$ Re = 5000–30000	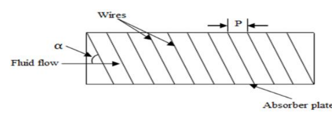	Gupta *et al.* [25]
Inclined with gap ribs	$P/e = 10$ $e/D_h = 0.0377$ $d/w = 0.167–0.5$ $g/e = 0.5–2.0$ Re = 5000–30000	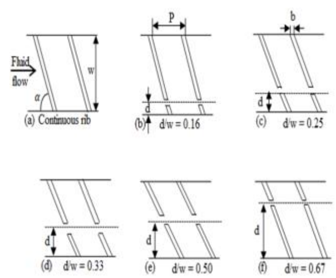	Aharwal *et al.* [32]
V-shaped continuous ribs	$P/e = 10$ $e/D_h = 0.020–0.034$ $\alpha = 30°–90°$ Re = 2500–18000	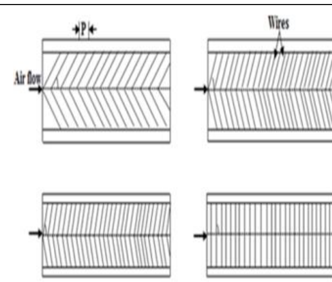	Momin *et al.* [33]
Multi v-shaped ribs	$P/e = 6–12$ $e/D_h = 0.019–0.043$ $W/w = 1–10$ $\alpha = 30°–75°$ Re = 2000–20000	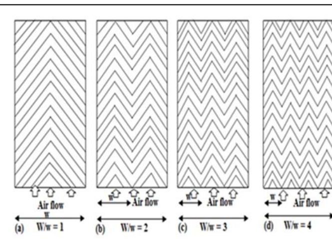	Hans *et al.* [30]

2 Experimental set-up and procedure

The experimental set-up has been elaborated to study the effect of rectangular duct SAH, adopting an alignment of multi-v and transverse wire ribs as a roughness geometry, on heat transfer and fluid flow characteristics. The three-side synthetically roughened SAH duct with a three-side lead crystal cover was investigated. At the same time, a one-side synthetically roughened SAH duct was also considered with only a top-side lead crystal cover. Figure 2 illustrates the three-side synthetically rugged solar air heater duct whereas Fig. 3 illustrates the one-side synthetically roughened SAH. The SAH ducts have a 200 mm × 25 mm flow cross-section as presented in Figs. 2 and 3.

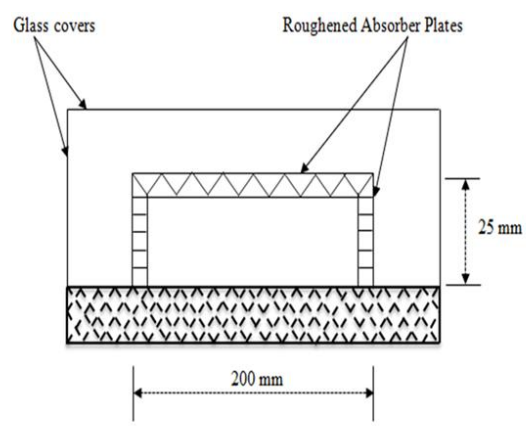

Figure 2: Three-side roughened solar air heater duct.

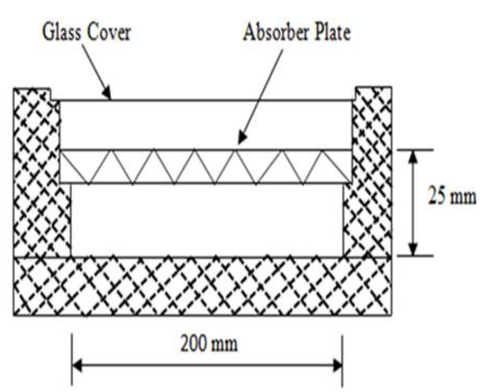

Figure 3: One-side roughened solar air heater duct.

Figures 4 and 5 demonstrate the roughened top and side absorber plates for three-side rugged SAHs having a galvanised iron (GI) sheet of 0.6 mm thickness. The photographic views are also shown in Figs. 6 and 7, respectively. The inner face of the remaining side of the duct is plane wooden. The duct was linked to a single blower to run accurately.

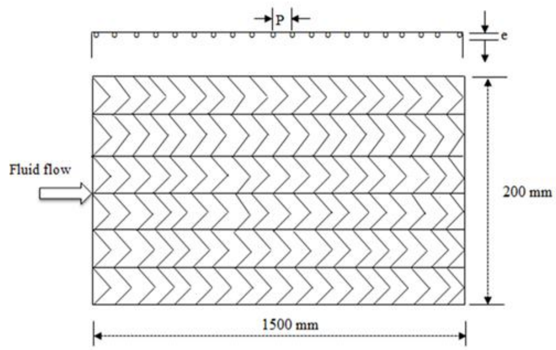

Figure 4: Top absorber plate for both 1-side and 3-side roughened SAH.

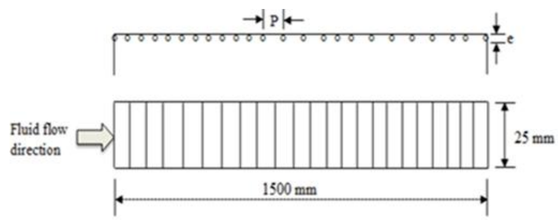

Figure 5: Side absorber plate for 3-side roughened SAH.

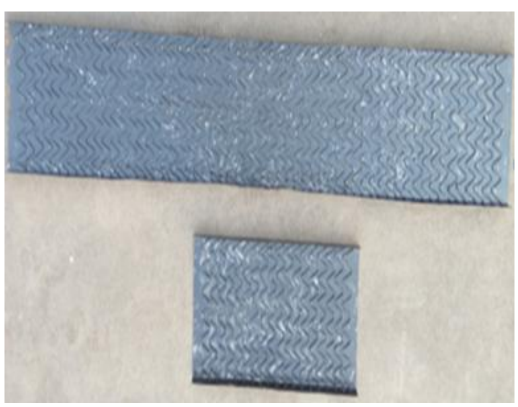

Figure 6: Photograph of the absorber plate for both 1-side and 3-side rugged SAHs.

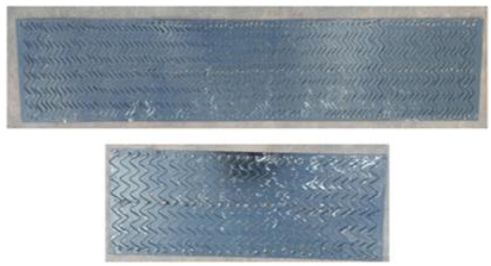

Figure 7: Photograph of top absorber plate for 1-side roughened SAHs.

The schematic presentation of the experimental set-up is shown in Fig. 8. It consists of an entry segment, test segment, a stream meter and a centrifugal blower. The two ducts, both one-side and three-side, are parallel in the measurement and are 2 m long, 0.2 m wide, and 0.025 m high. For both one-side and three-side synthetically rugged SAH ducts, only 1.5 m of duct length acts as the test segment and 0.5 m as the drift equalization bell-connected entrance segment. The solar collector entry segment was prohibited from solar emissions. Subsequently, the flow can be presumed to be absolutely established turbulent flow in the whole test segment length. The mass flow

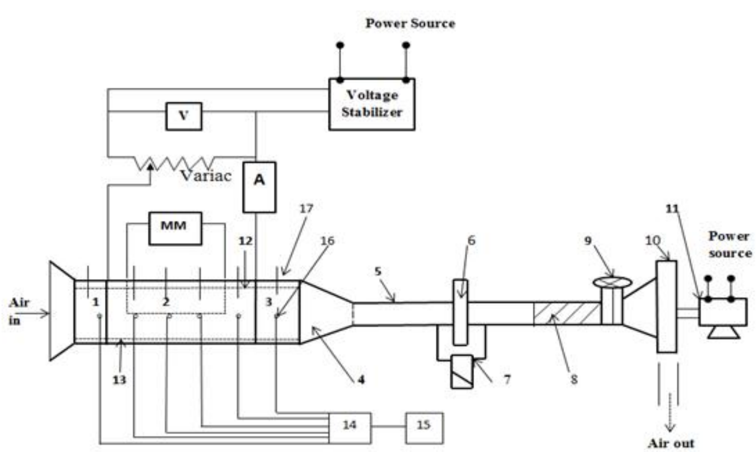

Figure 8: Schematic presentation of the experimental set-up: 1 – unheated entry section, 2 – heated test section, 3 – exit section, 4 – transition section, 5 – flow pipe, 6 – orifice meter, 7 – U-tube manometer, 8 – flexible pipe, 9 – gate valve, 10 – blower, 11 – electric motor, 12 – absorber plate, 13 – bottom of the duct, 14 – selectors switch, 15 – temperature recorder, 16 – thermocouple, 17 – digital thermometer, A – ammeter, MM – micromanometer, V – voltmeter.

rate of air in the duct was measured by a flange-tap orifice meter adapted in the stream channel; a blower using an auto-variac (variable transformer) associated with a stream tube for regulating the mass flow rate.

Figure 9 shows a photograph of the experimental set-up where a duct P is one-side rough, Q is the smooth duct and duct R is three-side roughened duct. To measure the fluid temperature, differential thermometers with a least count of 0.1 K were used, however, copper-constantan thermocouples of 28 SWG (British, Standard Wire Gage) were used for plate temperature measurements. Multi-tube manometers were linked to the pressure taps in the test segment ducts for measuring the pressure gradient. A digital pyranometer driven by a solar panel was used for distinguished measurements of the intensity of solar radiation, as shown in the photograph presented in Fig. 10.

Figure 9: Photographic representation of experimental set-up with three ducts.

Experimental data on heat transfer and friction factor was collected as per the recommendation of ASHRAE standard 93–97 (1977) [29] for the analysis of solar collector performance in an open loop flow mode. The data were gathered from the fluid side of the absorber plate for several arrangements of geometrical restrictions of the proposed synthetic rib roughness. Wood was chosen between other materials to construct the duct as it is cheap, easily obtainable and has also isolating properties. For the three-side roughened SAH, the top wall was set at four values of angle of attack ($\alpha = 30°$, 45°, 60°, and 75°) and side walls were perpendicular to the fluid stream direction at variable values of relative roughness pitch, P/e, in the range of 10–25, and relative roughness height, e/D_h, in the range of 0.018–0.042. The flow Reynolds number (Re) varied between 3000–12 000. At the initial

Figure 10: Photograph of digital pyranometer system.

stage of each measurement series, it was made sure that all measuring instruments work correctly and that there was no leakage at the joints. All measurements were made under steady-state conditions. For each measurement series, it takes 3–4 hours to reach the steady-state conditions from the start. The steady-state was expected to have been accomplished when no substantial deviation in the plate temperature and outlet air temperature was observed over a period of 15 minutes. The parameters recorded for each set were the following: inlet and outlet air temperature, absorber plate temperature at six points in the span-wise direction of the duct, trial section pressure head and orifice plate pressure gradient. In order to compare the performance of the three-side roughened SAH (top wall multi-v and two side walls transverse) versus one-side rugged SAH duct and the results of heat transfer and friction factor reported by Hans *et al.* [30], the ducts were tested under identical conditions.

3 Data collection and reduction

The experimental data were gathered from 12 arrangements of the roughened absorber plates and sixty tests for both one-side and three-side synthetically roughened SAHs simultaneously. The flow constraints remained identical for both categories of roughened SAHs for an individual test series, the records were made under the actual outdoor conditions. For a particular day, data were collected for an assumed mass stream rate under fluctuating values of intensity of solar radiation between 11:00 a.m. to 2:00 p.m. The hydraulic diameter for both SAH ducts is equal to 0.04444 m and the ducts are arranged in parallel. Some metrological data on a specific day are revealed in Table 2. The range of roughness and flow limitations are exposed in Table 3.

Table 2: Some metrological records

Metrological parameters	Time (hr)												
	11:00	11:15	11:30	11:45	12:00	12:15	12:30	12:45	13:00	13:15	13:30	13:45	14:00
Ambient temperature (°C)	35.8	36.5	36.7	36.9	37.5	38.3	38.6	38.9	39.4	39.7	39.9	40.0	40.1
Wind speed (m/s)	0.6	1.7	1.8	2.5	2.4	1.4	2.1	1.6	2.1	0.0	4.4	1.5	2.4
Ambient pressure $\times 10^2$ Pa	985.7	985.5	985.5	985.3	985.1	985.0	984.8	984.0	984.0	983.0	983.4	983.3	981.5
Total radiation (W/m^2)	878	892	903	903	898	879	868	844	821	808	790	761	729
Diffuse radiation (W/m^2)	279	281	282	287	281	284	288	286	286	271	279	2264	262
Direct radiation (W/m^2)	607	611	617	611	612	595	587	580	578	574	574	559	546
Normal radiation (W/m^2)	621	626	632	631	632	614	601	593	596	592	600	579	567
Relative humidity (%)	43	41	41	40	40	38	39	37	35	28	27	29	27

Table 3: Standards of roughness and flow restrictions

Parameter	Symbol	Values
Relative roughness pitch	P/e	10–25 (4 levels)
Relative roughness height	e/D_h	0.018–0.042 (4 levels)
Angle of attack	α	30°–75° (4 levels)
Relative roughness width	W/w	6 (1 level)
Reynolds number	Re	3500–12 000 (6 levels)

The experimental records for plate and air temperatures at several positions in the conduit were collected under steady-state conditions for a specified heat flux and mass stream rate of air. The information was used to compute the heat allocation rate to air streaming in the duct. In order to estimate the Nusselt number (Nu_r) and friction factor (f_r) the effect of roughness orientation and operating parameters on heat transfer and friction factor was investigated.

The consequent equations have been used for the estimation of mass flow rate ($\dot{m}$), useful heat gain (Q_u), heat transfer coefficient (h), Nusselt number (Nu_r), Reynolds number (Re) and friction factor (f_r). These equations were obtained by adopting experimental observations as described in the subsequent steps.

The mass stream rates have been determined from the pressure gradient measurement across the orifice plate:

$$\dot{m} = C_d A_o \left[\frac{2\rho \Delta P_o}{1-\beta^4}\right]^{0.5} . \tag{1}$$

The calibration of the orifice plate against a standard Pitot tube yielded the value of the discharge coefficient C_d as 0.624, where $P_o = g\rho_1 \Delta h_1$.

The rate of heat gain by the air and heat transfer coefficient for one-side and three-side synthetically roughened solar collectors can be determined by adopting a relationship

$$Q_u = \dot{m} C_p \left(t_o - t_i\right) = h A_p \left(t_p - t_f\right) . \tag{2}$$

The average value of plate temperature (t_p) was determined from the detailed temperature profile of the absorber plate indicated by six thermocouples at several positions:

$$t_p = \frac{t_{p1} + t_{p2} + t_{p3} + t_{p4} + t_{P5} + t_{p6}}{6} . \tag{3}$$

The average value of fluid temperature (t_f) was determined from the detailed temperature profile of air in the channel by six digital thermometers at several positions in the test section of the duct:

$$t_f = \frac{t_{f1} + t_{f2} + t_{f3} + t_{f4} + t_{f5} + t_{f6}}{6} . \tag{4}$$

The Reynolds number for the one-side and three-side roughened solar collector was calculated assuming an equation

$$\mathrm{Re} = \frac{\rho V D_h}{\mu} . \tag{5}$$

The Nusselt number for the one-side and three-side rugged solar collector was calculated assuming a relation

$$\mathrm{Nu}_r = \frac{hD_h}{k}\,. \tag{6}$$

The friction factor was determined from the flow velocity (v) and pressure drop (ΔP_d) through the test segment by applying the Darcy-Wiesbach equation:

$$f_r = \frac{2\Delta P_d D_h}{4\rho L V^2}\,, \tag{7}$$

where the hydraulic diameter $D_h = \dfrac{4WH}{2(W+H)}$, and the pressure drop across the duct is equal to

$$\Delta P_d = g\rho_2 \Delta h_2\,. \tag{8}$$

The absorber plate area (A_p) in Eq. (2) is different for the one-side and three-side rugged SAHs. It is equivalent to the top absorber plate area for the one-side rugged collector, whereas, it is the sum of the top collector area and two-side collector area for the three-side roughened solar air heater.

On the basis of error exploration carried out for different instruments used in measurement [13, 34], the uncertainties in the determination of several quantities are specified below:

1) the Reynolds number: ±1.04%,

2) the Nusselt number: ±2.57%,

3) the friction factor: ±2.26%.

4 Validity test

For validation purposes, the Nusselt number (Nu_r) and friction factor (f_r) were determined from testing on a multiple-v one-side rugged SAH duct with a fixed value of relative roughness pitch, $P/e = 10$, relative roughness height, $e/D_h = 0.042$, relative roughness width, $W/w = 6$, and angle of attack, $\alpha = 60°$. The respective results of the one-side roughened solar air heater were compared with results obtained from the correlations developed by Hans *et al.* [30]. For the Nusselt number and friction factor the following expressions were used:

$$\begin{aligned}\mathrm{Nu}_r = {} & 3.35 \times 10^{-5}\mathrm{Re}^{0.92}\left(\frac{e}{D_h}\right)^{0.77}\left(\frac{W}{w}\right)^{0.43}\left(\frac{\alpha}{90}\right)^{-0.49} \\ & \times \exp\left[-0.61\ln^2\left(\frac{\alpha}{90}\right)\right]\exp\left[-0.1177\ln^2\left(\frac{W}{w}\right)\right]\left(\frac{P}{e}\right)^{8.54} \\ & \times \exp\left[-2.0407\ln^2\left(\frac{P}{e}\right)\right],\end{aligned} \tag{9}$$

$$\begin{aligned}f_r = {} & 4.47 \times 10^{-4}\mathrm{Re}^{-0.3188}\left(\frac{e}{D_h}\right)^{0.73}\left(\frac{W}{w}\right)^{0.22}\left(\frac{\alpha}{90}\right)^{-0.39} \\ & \times \exp\left[-0.52\ln^2\left(\frac{\alpha}{90}\right)\right]\exp\left[-2.133\ln^2\left(\frac{P}{e}\right)\right]\left(\frac{P}{e}\right)^{8.9}.\end{aligned} \tag{10}$$

The comparison of values of (Nu_r) and (f_r) obtained from the present experimental work and the work of Hans *et al.* [30] is illustrated in Figs. 11 and 12, respectively. The discrepancy of the obtained experimental values for (Nu_r) is ±2.3% with respect to the theoretical values given in Eq. (9). At the same time, the discrepancy of the obtained experimental values for the friction factor is ±2.27% from the theoretical values given by Eq. (10). This illustrates a good agreement between experimental and theoretical

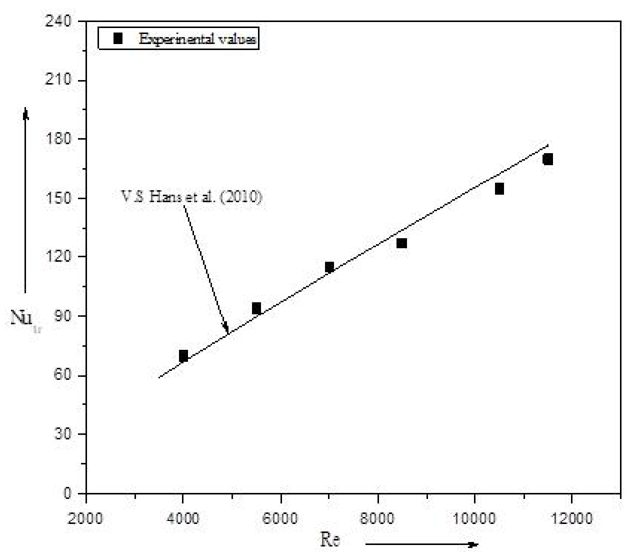

Figure 11: Nusselt number validation.

values, which certifies the correctness of performance of the composed experimental set-up.

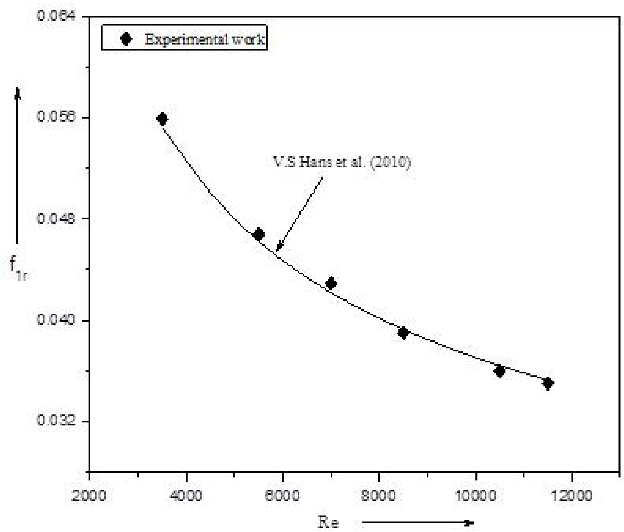

Figure 12: Friction factor validation.

5 Results and discussion

The heat transfer and friction characteristics of the three-side roughened rectangular duct SAH with the combination of multiple-v and transverse wire (top wall multi-v and two side walls transverse), computed on the basis of experimental data gathered for several flow and roughness restrictions are discussed below. These results are compared with those achieved for the case of one-side rugged duct SAH having fixed values of relative roughness pitch, $P/e = 10$, relative roughness height, $e/D_h = 0.042$, angle of attack, $\alpha = 60°$, and relative roughness width, $W/w = 6$, working under parallel circumstances. Figure 13 illustrates the intensity of solar emission and ambient air temperature during a specific day. Figure 14 displays the variation of the plate and air temperature in three-side and one-side roughened SAHs, associated with the variation of the fluid inlet temperature and solar emission. As might be realised from Fig. 13, the ambient temperature changes slowly with time whereas the intensity of solar emission rises up to 11:30 a.m., then decreases abruptly. Figure 14 indicates that both the plate and air temperature are greater in the three-side roughened collector as related to the one-side roughened collector. Figure 15 displays the change of the mean plate and fluid temperature with the intensity of solar emission. Again both parameters are greater in the three-side roughened SAH as compared to the one-side roughened SAH.

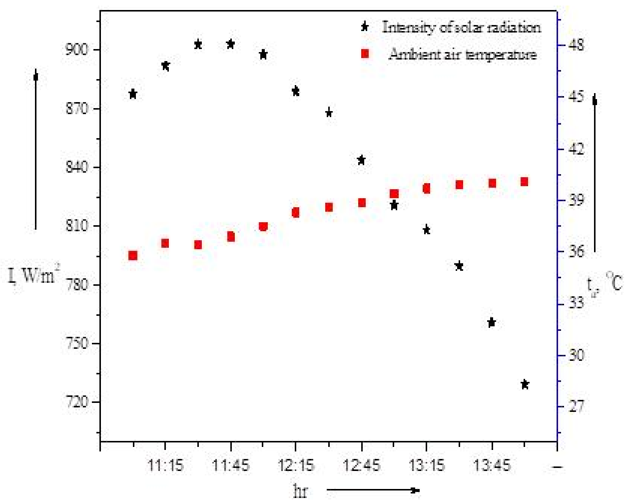

Figure 13: Intensity of solar emission and ambient air temperature during a specific day.

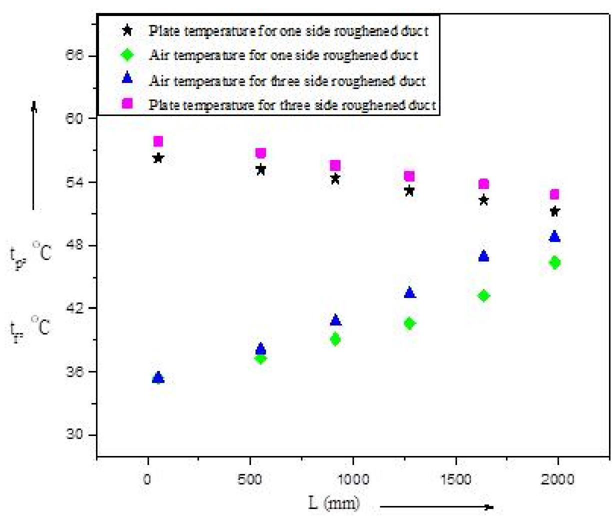

Figure 14: Plate and fluid temperature.

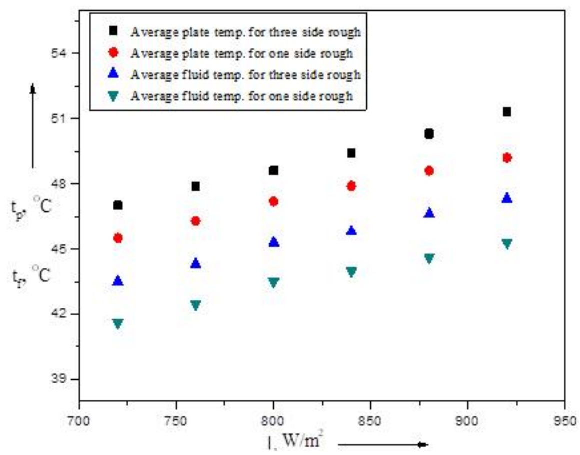

Figure 15: Average plate and fluid temperature.

5.1 Comparison of heat transfer and friction factor data

Figure 16 exhibits the comparison of the relevant Nusselt numbers for the one-side and three-side rugged duct SAHs obtained during the present experimental work and those of Hans *et al.* [30]. The evaluation of heat transfer data made for given values of relative roughness pitch, $P/e = 10$, relative roughness height, $e/D_h = 0.042$, angle of attack, $\alpha = 60°$, and fixed value of $W/w = 6$, for the stream Reynolds number Re = 3500–12 000. The ex-

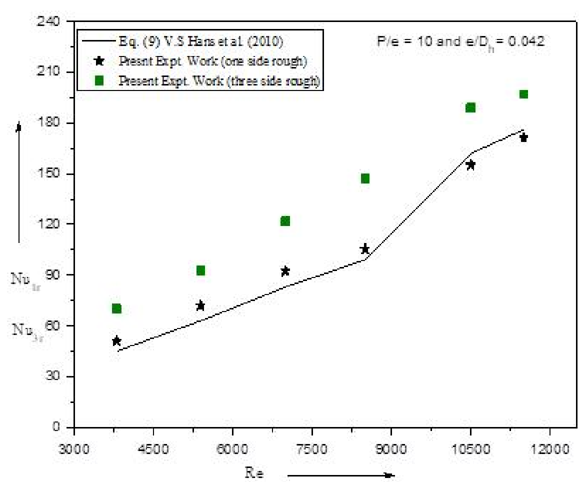

Figure 16: Comparison of Nu_r data for $e/D_h = 0.042$.

perimental values of Nu_r in the three-side rugged SAH are greater with respect to the one-side rugged SAH. In the same way, Fig. 17 illustrates the change of heat transfer characteristics for given values of $P/e = 10$ and $e/D_h = 0.034$, showing a similar trend with the increasing Reynolds number.

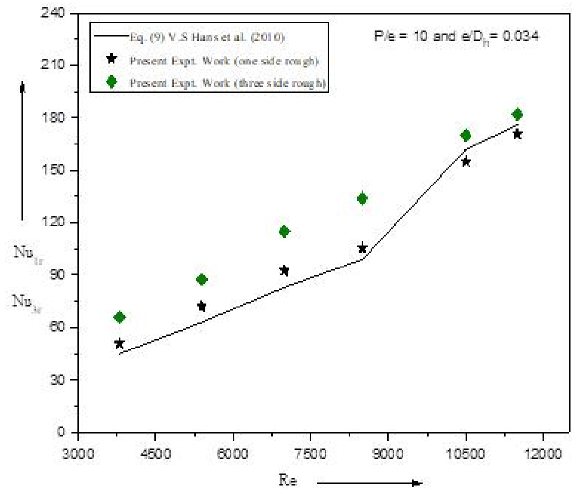

Figure 17: Comparison of Nu_r data for $e/D_h = 0.034$.

Figures 18 and 19 show the assessment of the friction factor for the three-side roughened solar air heater and one-side roughened solar air heater

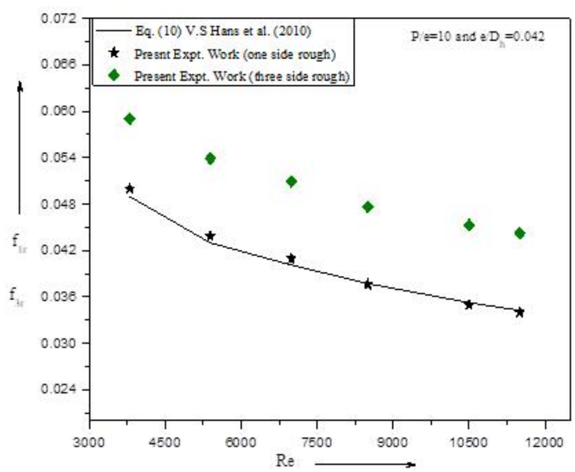

Figure 18: Comparison of f_r data for $e/D_h = 0.042$.

obtained during the present experimental work and a comparison with the results of Hans *et al.* [30]. As can be seen, the three-side solar air heater is characterized by a greater value of friction factor as compared to the one-side roughened solar air heater. The friction factor is also found to increase with the increasing value of relative roughness height.

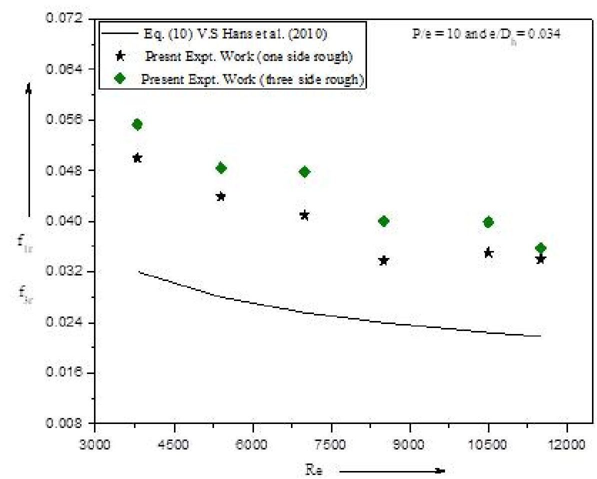

Figure 19: Comparison of f_r data for $e/D_h = 0.034$.

5.2 Other Nusselt number and friction factor data

Figures 20 and 21 are presented to realise the influence of roughness and flow restrictions on heat transfer intensification in the three-side roughened SAH as compared to the one-side roughened SAH. Figure 20 illustrates the impact of relative roughness pitch, P/e, on the Nusselt number, Nu_{3r}, for the three-side rugged collector and Nu_{1r} for the one-side rugged collector, for given values of relative roughness height, $e/D_h = 0.042$, and angle of attack, $\alpha = 60°$, within a range of Reynolds numbers. Figure 21 exhibits the effect of relative roughness height, e/D_h, on Nu_{3r} for the three-side roughened collector and Nu_{1r} for the one-side roughened collector, for a given value of relative roughness pitch, $P/e = 10$, and angle of attack, $\alpha = 60°$, within the investigated range of Reynolds numbers. The Nusselt number Nu_{3r} for the three-side roughened collector is increased by an extent of 24–76% over that of Nu_{1r} for the one-side roughened collector.

Figures 22 and 23 illustrate the effect of flow restrictions on friction factor in the three-side roughened and one-side roughened SAHs. Figure 22

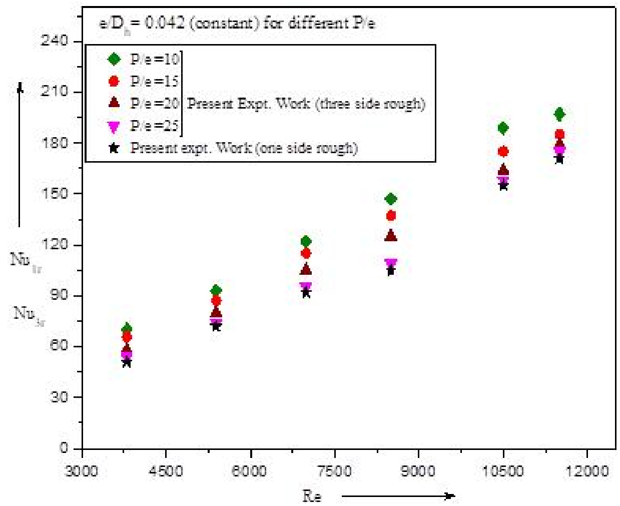

Figure 20: Effect of P/e on Nu_{1r} in three-side roughened SAHs.

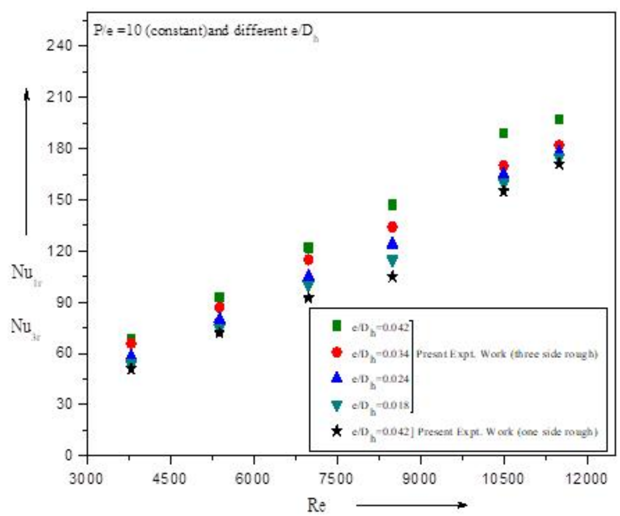

Figure 21: Effect of e/D_h on Nu_r in three-side rugged SAHs.

exhibits the impact of relative roughness pitch, P/e, on the friction factor f_{3r} for the three-side roughened collector and f_{1r} for the one-side roughened collector, for given values of relative roughness height, $e/D_h = 0.042$, and angle of attack, $\alpha = 60°$, for a given range of Reynolds numbers. Figure 23 illustrates the effect of relative roughness height, e/D_h, on the friction factor

f_{3r} for the three-side roughened collector and f_{1r} for the one-side roughened collector, for given values of relative roughness pitch, $P/e = 10$, and angle of attack, $\alpha = 60°$, for a given range of Reynolds numbers. The values of friction factor f_{3r} in the three-side roughened collector exceed by 4–36% those of f_{1r} for the one-side roughened collector.

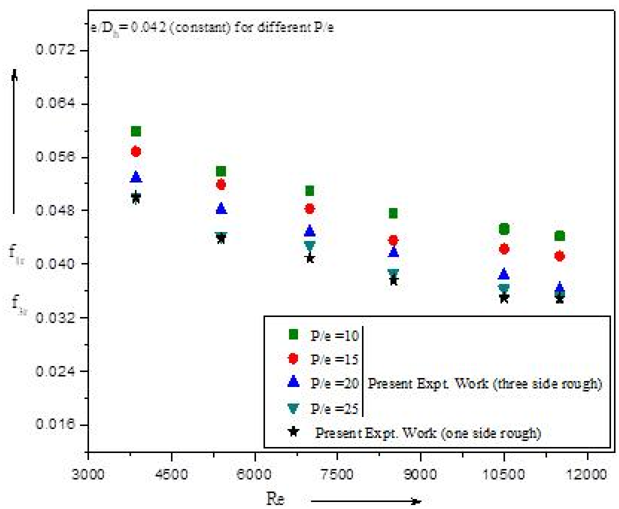

Figure 22: Effect of P/e on f_r in three-side roughened SAHs.

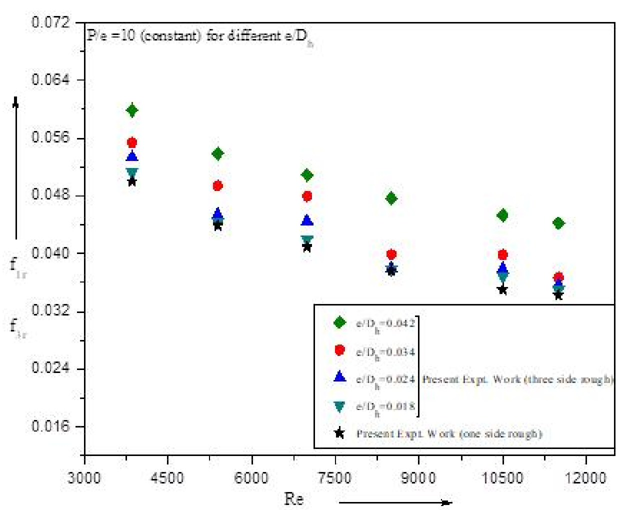

Figure 23: Effect of e/D_h on f_r in three-side roughened SAHs.

5.3 Heat transfer enhancement

The heat transfer coefficient in the three-side artificially roughened SAH is greater as compared to the one-side roughened SAH. Figure 24 illustrates the heat transfer enhancement ratio, (Q_{3r}/Q_{1r}), versus the intensity of solar radiation, at varying values of Re, for a fixed angle of attack, $\alpha = 60°$. The following equations have been adopted for Q_{3r} and Q_{1r}:

$$Q_{3r} = h_{3r} A_{p3r} \Delta t_3 \,, \tag{11}$$

$$Q_{1r} = h_{1r} A_{p1r} \Delta t_1 \,. \tag{12}$$

It might be realised that the heat transfer enhancement ratio increases with the rising value of Reynolds number and the increasing intensity of solar emission. The three-side roughened SAHs are thermally superior over the one-side roughened SAHs; their performance is also boosted at larger Reynolds numbers and larger intensities of solar radiation.

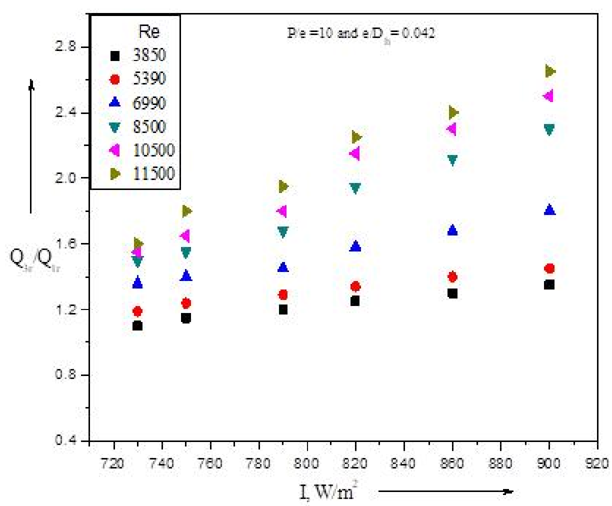

Figure 24: Heat transfer enhancement ratio.

6 Conclusions

Based on the experimental exploration of heat transfer and friction factor in the three-side artificially roughened rectangular duct SAHs with an arrangement of multiple-v (top wall multi-v and two side walls transverse), the following conclusions can be drawn:

- The value of Nusselt number increases whereas the friction factor drops as the Reynolds number increases.
- The Nusselt number and friction factor increase with the increasing value of relative roughness height (e/D_h) and decreases with the increasing value of relative roughness pitch (P/e).
- The Nusselt number and friction factor in three-side artificially roughened SAHs are increased by 24–76% and 4–36%, respectively, over those of one-side roughened SAHs for similar operating conditions.
- The maximum value of heat transfer enrichment ratio for the three-side roughened SAH with respect to the one-side roughened SAH is found to be 2.80.
- Three-side artificially rugged SAHs are superior as compared to one-side artificially roughened SAHs qualitatively and quantitatively.

Received 15 May 2022

References

[1] Bhatti M.S., Shah R.K.: *Turbulent and Transition Flow Convective Heat Transfer Handbook of Single Phase Convective Heat Transfer*. Wiley, New York 1987.

[2] Garg H.P., Prakash J.: *Solar Energy Fundamentals and Applications* (1st Edn.). Tata McGraw-Hill, New Delhi 2000.

[3] Kumar D., Prasad L.: *Performance analysis of three side's solar air heater having roughness elements as a combination of multiple-v and transverse wire on the absorber plate*. Arch. Thermodyn. **41**(2020), 3, 125–146.

[4] Al-Joboory H.N.S.: *Experimental and theoretical investigation of an evacuated tube solar water heater incorporating wickless heat pipes*. Arch. Thermodyn. **41** (2020), 3, 3–31.

[5] Menni Y., Chamkha A.J., Zidani C., Benyoucef B.: *Analysis of thermo-hydraulic performance of a solar air heater tube with modern obstacles*. Arch. Thermodyn. **41**(2020), 3, 33–56.

[6] Kumar V.: *Augmentation in heat transfer and friction of three sides over one side dimple roughened solar duct*. Arch. Thermodyn. **41**(2020), 3, 57–89.

[7] Sahu M.K., Matheswaran M.M., Bishnoi P.: *Experimental investigation of augmented thermal and performance characteristics of solar air heater ducts due to varied orientations of roughness geometry on the absorber plate*. Arch. Thermodyn. **41**(2020), 3, 147–182.

[8] Ghritlahre H.K., Sahu P.K.: *A comprehensive review on energy and exergy analysis of solar air heaters.* Arch. Thermodyn. **41**(2020), 3, 183–222.

[9] Ghritlahre H.K., Chandrakar P., Ahmad A.: *Solar air heater performance prediction using artificial neural network technique with relevant input variables.* Arch. Thermodyn. **41**(2020), 3, 255–282.

[10] Ghritlahre H.K.: *An experimental study of solar air heater using arc shaped wire rib roughness based on energy and exergy analysis.* Arch. Thermodyn. **41**(2021), 3, 115–139.

[11] Kumar V., Prasad L.: *Thermal performance investigation of three side's concave dimple roughened solar air heaters.* Sol. Energy **188**(2019), 361–379.

[12] Kumar D., Prasad L.: *Analysis on optimal thermohydraulic performance of solar air heater having multiple V-shaped wire rib roughness on absorber plate.* Int. Energy J. **18**(2018), 153–170.

[13] Holman J.P.: *Experimental Method for Engineers.* McGraw-Hill, New York 2007.

[14] Prasad B.N.: *Thermal performance of artificially roughened solar air heaters.* Sol. Energy **91**(2013), 59–67.

[15] Prasad B.N., Saini J.S.: *Effect of artificial roughness on heat transfer and friction factor in a solar air heater.* Sol. Energy **41**(1988), 6, 555–60.

[16] Kumar D., Prasad L.: *Heat transfer augmentation of various roughness geometry used in solar air heaters.* Int. J. Mech. Eng. Technol. **12**(2017), 8, 491–508.

[17] Zidani C., Benyoucef B., Didi F., Guendouz, N.: *Simulation and numerical analysis of a rectangular pipe with transversal baffle – comparison between zigzag and plane baffles.* Arch. Thermodyn. **41**(2020), 4, 269–283.

[18] Kumar D., Prasad L.: *Thermo-hydraulic performance of solar air heater having multiple V-shape rib on absorber plates.* Carbon-Sci. Tech. **10**(2018), 1, 39–50.

[19] Daghsen K., Lounissi, D., Bouaziz, N.: *A universal model for solar radiation exergy accounting: Case study of Tunisia.* Arch. Thermodyn. **43**(2022), 2, 97–118.

[20] Kumar A., Layek A.: *Energetic and exergetic performance evaluation of solar air heater with twisted rib roughness on absorber plate.* J. Clean. Prod. **232** (2019), 617–628.

[21] Behura A.K., Prasad B.N., Prasad L.: *Heat transfer friction factor and thermal performance of three sides artificially roughened solar air heaters.* Sol. Energy **130**(2016), 46–59.

[22] Karwa R., Chitoshiya G.: *Performance study of solar air heater having v-down discrete ribs on absorber plate.* Energy **55**(2013), 939–955.

[23] Kumar A., Saini R.P., Saini J.S.: *Development of correlations for Nusselt number and friction factor for solar air heater with roughened duct having multi v-shaped with gap ribs as artificial roughness.* Renew. Energ. **58**(2013), 151–163.

[24] Maithani R., Saini J.S.: *Heat transfer and friction factor correlations for a solar air heater duct artificially with v-ribs with symmetrical gaps.* Exp. Therm. Fluid Sci. **70**(2016), 220–227.

[25] Gupta D., Solanki S.C., Saini J.S.: *Thermohydraulic performance of solar air heaters with roughened absorber plates.* Sol. Energy **61**(2000), 33–42.

[26] Deo N.S., Chander S., Saini J.S.: *Performance analysis of solar air heater duct roughened with multigap V-down ribs combined with staggered ribs*. Renew. Energ. **91**(2016), 484–500.

[27] Prasad B.N., Behura A.K., Prasad L.: *Fluid flow and heat transfer analysis for heat transfer enhancement in three sided artificially roughened solar air heater*. Sol. Energy **105**(2014), 27–35.

[28] Singh S., Chander S., Saini J.S.: *Thermal and effective efficiency based analysis of discrete V down rib roughened solar air heaters*. J. Renew. Sust. Energ. **3**(2011), 023107–023126.

[29] American Society of Heating, Refrigerating and Air-Conditioning Engineers: *Method of Testing to Determine the thermal performance of solar collectors* (ASHRAE Standard 93-97). New York 1977.

[30] Hans V.S., Saini R.P., Saini J.S.: *Heat transfer and friction factor correlations for a solar air heater duct roughened artificially with multiple v-ribs*. Sol. Energy **84**(2010), 898–911.

[31] Kumar A., Saini R.P., Saini J.S.: *Experimental Investigation on heat transfer and fluid flow characteristics of air flow in a rectangular duct with multi v-shaped rib with gap roughness on the heated plate*. Sol. Energy **86**(2012), 1733–1749.

[32] Aharwal K.R., Gandhi B.K., Saini J.S.: *Experimental investigation on heat transfer enhancement due to a gap in an inclined continuous rib arrangement in a rectangular duct of solar air heater*. Renew. Energ. **33**(2008), 585–596.

[33] Momin A.M.E., Saini J.S., Solanki S.C.: *Heat transfer and friction in solar air heater duct with v-shaped rib roughness on absorber plate*. Int. J. Heat Mass Tran. **45**(2002), 3383–3396.

[34] Kline S.J., Mcclintok F.A.: *Describing uncertainties in single sample experiment*. Mech. Eng. **75**(1953), 1, 3–8.